Radiative Noise Reduction Technique using 12 Coils Suitable for High-power Inductive Power Transfer

Keisuke Kusaka
Dept. of Electrical, Electronics and Information Engineering
Nagaoka University of Technology
Nagaoka, Niigata, Japan
kusaka@vos.nagaokaut.ac.jp

Keita Furukawa
Dept. of Electrical, Electronics and Information Engineering
Nagaoka University of Technology
Nagaoka, Niigata, Japan
archer_FK@stn.nagaokaut.ac.jp

Jun-ichi Itoh
Dept. of Science of Technology Innovation
Nagaoka University of Technology
Nagaoka, Niigata, Japan
itoh@vos.nagaokaut.ac.jp

***Abstract*—High power inductive power transfer system for electrical vehicles is highly requested today in order to shorten a charging time of an onboard battery. One of the difficulties of increasing power is radiation noise. The radiation noise may greatly increase as transmission power increase. The radiation noise must satisfy a regulation, which is/will be legislated. In this paper, an inductive power transfer system with 12 solenoid coils is proposed to suppress the radiation noise. The proposed 12-coils IPT system has six coils on a primary side and six coils on a secondary side. The six coils on the primary side are circularly placed in every 60 degrees in order to cancel out the radiation noise and magnetic interference among the six coils. The two opposed solenoid coils cancel out the radiative noise because these coils generate flux in the opposite direction. Moreover, the magnetic coupling among six coils with three-phase equilibrium current cancels out the magnetic interference, which degrades a power factor of the inductive power transfer system. The six coils on the secondary side are placed in the same manner. The proposed IPT system is tested with a 2.9-kW prototype. The radiative noise on the fundamental frequency is suppressed by 1/6 using the proposed 12-coil system. Moreover, the calculated power loss shows good agreement with the measured power loss with an error of 7.3%.**

Keywords—inductive power transfer, wireless power transfer, magnetic interference, three-phase transmission

I. INTRODUCTION

In recent years, inductive power transfer (IPT) systems for electrical vehicles (EVs) have been actively studied [1-4]. The IPT systems transmit power using magnetic coupling between coils without an electric cable. Thus, the IPT systems will improve the usability of the EVs because users of EVs do not need to connect the wire when they charge an onboard battery. Currently, the development of the IPT system with an input power of 3.3 kW or 7.7 kW are ongoing towards a commercial realization for the light-duty vehicles with a standard, which will be published by ISO/IEC [5–6]. In the standard, the IPT system is classified by the input power. The IPT system with an input power of less than 3.3 kW and 7.7kW are WPT1 and WPT2, respectively.

Meanwhile, the amount of the onboard battery of EVs tends to increase in order to extend a travel distance. As a wired fast charging system, an output power of 50 kW or more is required. Additionally, the power of the wired charger is planned to be increased to 150 kW or 350 kW in CHAdeMO. The output power of the IPT system should be increased for the quick charge with considering the trend of increasing power of the EV charger. As high power IPT systems, WPT3, WPT4, and WPT5 will be standardized [5–6]. The maximum input power P_{in} of WPT 3 is 7.7 kW < P_{in} ≤ 11 kW, WPT4 is 11 kW < P_{in} ≤ 22 kW, and WPT5 is P_{in} > 22 kW will be standardized.

One of the challenges of increasing power is a radiation noise, which is emitted by the transmission coils. The magnetic flux from the coil is in proportional to the current on the coils. Then, the radiation noise will increase as the output power increase. The radiation noise may cause the malfunction of electrical equipment and jam a radio communication. Thus, the radiation noise from the IPT system must be suppressed to below the allowable level, which will be legislated in each area or countries. Note that, this allowable level is determined based on the CISPR's guideline [7].

In [8], radiation noise reduction technique using a spread spectrum is proposed. The peak of the radiation noise on the fundamental frequency and low-order harmonic frequencies are suppressed by changing the transmission frequency at every period. Especially, a new spread spectrum method, which selects the transmission frequency using a biased probability distribution, is proposed in [8]. The radiation noise is suppressed by only changing the control of the primary inverter. However, the effect of the suppression performance is not enough for the high power IPT system.

Meanwhile, the radiation noise reduction technique with four solenoid coils has been proposed [9]. The pair of the primary coils is placed to cancel out the radiation noise. The secondary coils are in the same manner. From the theoretical analysis, the maximum performance on the noise reduction is obtained when the two coils are placed to face each other. However, the magnetic coupling, which is also called as magnetic interference, between the two coils causes a circulating current. It limits the freedom of the coil placement because the circulating current increases a copper loss.

This paper proposes a three-phase inductive power transfer system with 12 coils. The proposed system has six solenoid coils for the primary side and six solenoid coils for the secondary side. The six pairs of the coils on each side are circularly placed in every 60 degrees. The opposed coils cancel out the radiation noise because countercurrent flows on the two coils. The opposed coils are the best placement to cancel out the radiation noise [9]. Moreover, the six coils cancel out the magnetic interference among these coils when the equilibrium current flow on the coils. Due to this coil structure, the three-phase IPT system without magnetic interference among the coils is obtained. In other words, six IPT systems, which are magnetically independent of each other, is achieved. In this paper, first, a system configuration of the three-phase IPT system is explained. Next, a design procedure to cancel out the magnetic interference is described. Then, the experimental results about the radiation noise and power loss distribution with a 2.9-kW prototype is shown. Finally, a 22-kW IPT system is designed for WPT5.

II. Proposed IPT System with 12 Coils

In this chapter, the proposed three-phase IPT system is introduced. The proposed system achieves cancellation of the radiation noise and magnetic interference among 12 coils by a special coil structure and three-phase equilibrium current.

A. System Configuration

Figure 1 shows the three-phase inductive power transfer system. The proposed system consists of the three-phase inverter, resonant capacitors, six primary coils, six secondary coils, and three-phase rectifier. The three-phase inverter is operated in square wave operation at around 85 kHz. The phase difference among the phase are 120 degrees.

The resonant capacitors are inserted to the output of the inverter and the input of the rectifier on each phase in series for compensation of a reactive power, which is caused by weak magnetic coupling between the primary coil and the secondary coil. This topology is as same as the series-series compensation [11], which is typically used for a single-phase IPT. The design of the capacitors is explained in the next section.

The six primary and six secondary coils are connected in star-star connection. Power is transmitted through the three-phase windings. Note that, the coils can be connected in star-delta, delta-star, and delta-delta connection. However, the explanation of these connections is omitted in this paper due to the page limitation. In this system, the two coils L_{xnA} and L_{xnB} are connected in series in the phase, where suffix "x" represent "u," "v," or "w," and n is "1" or "2" for representing the primary or secondary side. These series-connected coils cancel out the magnetic raditaion because these coils are placed in the opposite. However, the coils L_{xnA} and L_{xnB}, which are magnetically coupled, causes the magnetic interference. The magnetic interference should be canceled out with the coil structure because the magnetic interference degrades the power factor reflected from the inverter output. The cancellation technique will be explained in the next section.

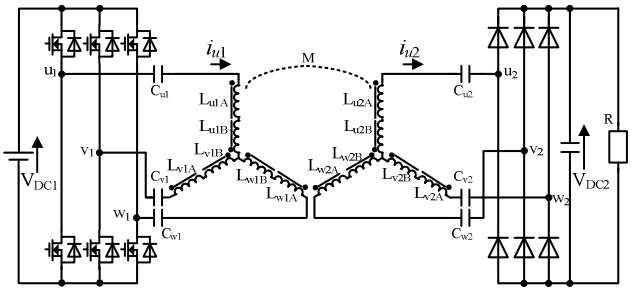

Fig. 1. Three-phase inductive power transfer system with six primary coils and six secondary coils. The six coils in each side are connected in star winding.

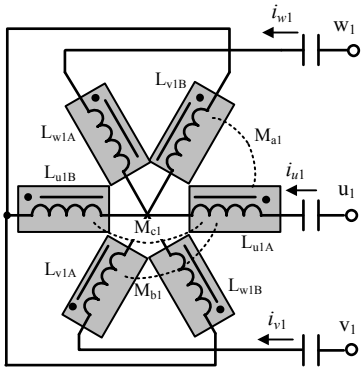

Fig. 2. Coil placement and connection.

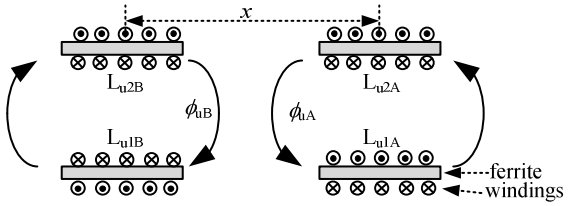

Fig. 3. Mechanism of radiation noise reduction with two pairs of solenoid coils.

Figure 2 shows the placement of the 12 coils and the connection. In the proposed system, the solenoid-coils are circularly placed. The secondary coils are put onto the primary coils across the air gap. The power is transmitted from the bottom coils to the upper coils, e.g., L_{u1A} to L_{u2A} with a mutual coupling M.

$$\begin{pmatrix} v_{u1A} \\ v_{u1B} \\ v_{v1A} \\ v_{v1B} \\ v_{w1A} \\ v_{w1B} \\ v_{u2A} \\ v_{u2B} \\ v_{v2A} \\ v_{v2B} \\ v_{w2A} \\ v_{w2B} \end{pmatrix} = \begin{pmatrix} L_{1Ys} & M_{c1} & M_{b1} & M_{a1} & M_{b1} & M_{a1} & M & 0 & 0 & 0 & 0 & 0 \\ M_{c1} & L_{1Ys} & M_{a1} & M_{b1} & M_{a1} & M_{b1} & 0 & M & 0 & 0 & 0 & 0 \\ M_{b1} & M_{a1} & L_{1Ys} & M_{c1} & M_{b1} & M_{a1} & 0 & 0 & M & 0 & 0 & 0 \\ M_{a1} & M_{b1} & M_{c1} & L_{1Ys} & M_{a1} & M_{b1} & 0 & 0 & 0 & M & 0 & 0 \\ M_{b1} & M_{a1} & M_{b1} & M_{a1} & L_{1Ys} & M_{c1} & 0 & 0 & 0 & 0 & M & 0 \\ M_{a1} & M_{b1} & M_{a1} & M_{b1} & M_{c1} & L_{1Ys} & 0 & 0 & 0 & 0 & 0 & M \\ M & 0 & 0 & 0 & 0 & 0 & L_{2Ys} & M_{c2} & M_{b2} & M_{a2} & M_{b2} & M_{a2} \\ 0 & M & 0 & 0 & 0 & 0 & M_{c2} & L_{2Ys} & M_{a2} & M_{b2} & M_{a2} & M_{b2} \\ 0 & 0 & M & 0 & 0 & 0 & M_{b2} & M_{a2} & L_{2Ys} & M_{c2} & M_{b2} & M_{a2} \\ 0 & 0 & 0 & M & 0 & 0 & M_{a2} & M_{b2} & M_{c2} & L_{2Ys} & M_{a2} & M_{b2} \\ 0 & 0 & 0 & 0 & M & 0 & M_{b2} & M_{a2} & M_{b2} & M_{a2} & L_{2Ys} & M_{c2} \\ 0 & 0 & 0 & 0 & 0 & M & M_{a2} & M_{b2} & M_{a2} & M_{b2} & M_{c2} & L_{2Ys} \end{pmatrix} \frac{d}{dt} \begin{pmatrix} i_{u1} \\ -i_{u1} \\ i_{v1} \\ -i_{v1} \\ i_{w1} \\ -i_{w1} \\ i_{u2} \\ -i_{u2} \\ i_{v2} \\ -i_{v2} \\ i_{w2} \\ -i_{w2} \end{pmatrix} \tag{1}$$

Fig. 3 shows the principle of the radiation noise reduction with two coils. The two coils on common phase such as L_{u1A} and L_{u1B} are differentially connected and placed in the opposite. For this reason, the flux, which is generated from the coils, is the opposite direction and the same flux amplitude. Thus, the radiation noise is canceled out at the measuring point, which is typically 10 m from the system [7]. The principle of the cancellation is explained in detail in [9–10].

The remaining two pairs of the coils on phase-v and phase-w are placed in every 120 degrees to the coils on phase-u. In the IPT system with multiple coils, the magnetic interference occurs. In this system, there are three kind of magnetic interference M_a, M_b, and M_c due to the symmetrical placement of coils. M_a is the mutual coupling between the adjacent coils, e.g., L_{u1A} and L_{v1B}. M_b is the mutual coupling between the coils apart from 120 degrees, e.g., L_{u1A} and L_{v1A}. M_c is the mutual coupling between the opposed coils, e.g., L_{u1A} and L_{u1B}. By adjusting these magnetic interference, the effect of the magnetic interference is canceled out. In other words, six single-phase IPT systems, which are magnetically independent of each other, with radiation noise reduction capability are achieved.

B. Cancellation of Effect by Magnetic Interference

In this subsection, the cancellation method of the effect by the magnetic interference among the coils M_a, M_b, and M_c is explained. As shown in the previous subsection, the proposed system has three kinds of the magnetic interference. These magnetic interference increase circulating current among the coils. The effect of the magnetic interference should be suppressed since the circulating current decrease the transmission efficiency.

Equation (1) represents the induced voltage v_{xn} on each coil, where L_{nYs} are the self-inductance of each coil, M is the main mutual coupling, and i_{xn} are the current on each coil. The mutual coupling contributes to transmits power from the primary side to the secondary side. Focusing on the first line of (1), the induced voltage on the coil L_{u1A} is expressed by

$$\begin{aligned} v_{u1A} = {} & L_{1Ys}\frac{di_{u1}}{dt} + M\frac{di_{u2}}{dt} - M_{c1}\frac{di_{u1}}{dt} \\ & - M_{a1}\left(\frac{di_{v1}}{dt} + \frac{di_{w1}}{dt}\right) + M_{b1}\left(\frac{di_{v1}}{dt} + \frac{di_{w1}}{dt}\right) \end{aligned} \tag{2}$$

In (1), the first term is the induced voltage by the self-inductance, the second term is the induced voltage by the mutual inductance, which contributes transmitting power. Although, the third to fifth terms in (1) is the induced voltage by the magnetic interference. In other words, the effect of the magnetic interference can be zero if the sum of the third to fifth terms is zero.

The primary current can be expressed as (3) when the three-phase current is an equilibrium where ω is the angular transmission frequency, I_{m1} is the amplitude of the primary current.

$$\left\{ \begin{aligned} i_{u1} &= I_{m1}\sin\omega t \\ i_{v1} &= I_{m1}\sin\left(\omega t - \frac{2}{3}\pi\right) \\ i_{w1} &= I_{m1}\sin\left(\omega t - \frac{4}{3}\pi\right) \end{aligned} \right\} \tag{3}$$

Substituting (3) into (2), (2) is transformed to

$$\begin{aligned} v_{u1A} = {} & L_{1Ys}\frac{di_{u1}}{dt} + M\frac{di_{u2}}{dt} \\ & - \omega I_m \left\{ M_{c1}\cos\omega t + (M_{a1} - M_{b1})\cos\left(\omega t - \frac{2}{3}\pi\right) \right. \\ & \left. (M_{a1} - M_{b1})\cos\left(\omega t - \frac{4}{3}\pi\right) \right\} \end{aligned} \tag{4}$$

From (4), the condition for the cancellation of the magnetic interference is derived. The induced voltage caused by the magnetic interference is zero when

$$M_{a1} = M_{b1} + M_{c1} \tag{5}$$

is satisfied. The self-inductance of the primary coils are common. Thus, (5) can be expressed as

$$k_{a1} = k_{b1} + k_{c1} \tag{6}$$

Therefore, the unwanted induced voltages, which are caused by the magnetic interference is canceled by adjusting the magnetic coupling among the primary coils.

In the same manner, the cancellation condition on the secondary side can be introduced from the seventh line of (1) as

$$k_{a2} = k_{b2} + k_{c2} \tag{7}$$

The transmission coils should be designed to satisfy (6–7).

Figure 4 shows the simulated effect of the magnetic interference on the power factor reflected from the inverter output. The dotted line in these graphs is the cancellation condition of the magnetic interference calculated by (6–7). When the three magnetic interferences are negligible, the power factor is unity. However, the power factor greatly degrades when only one or two magnetic interference increase. However, if the three magnetic interference increases along the dotted line, the power factor remain high. From these graphs, the validity of the cancellation condition of the magnetic interference is confirmed.

III. Design and Analysis of Three-phase IPT System

A. Parameter Design

The proposed IPT system is designed in this chapter under the assumption that the magnetic interference is canceled out by satisfying (6–7).

First, the equivalent AC resistance should be calculated. The AC resistance R_{eq} is derived by expanding a derivation method of an equivalent AC resistance of a single-phase rectifier described in [12]. The equivalent resistance of the capacitor-input three-phase rectifier is calculated by

$$R_{eq} = \frac{8}{\pi^2}\frac{\left(V_{DC2}/2\right)^2}{P/3} = \frac{6}{\pi^2}\frac{V_{DC2}^2}{P} \tag{8},$$

where V_{DC2} is the secondary voltage at rated power and P is the rated output power. Note that the resistance is for one phase.

Next, the secondary inductance is designed in order to maximize transmission efficiency. From the impedance matching perspective, the impedance of the secondary inductance should be equal to the load, i.e., AC equivalent resistance derived by (8). Note that the winding resistance is ignored for the simplicity. Thus, the secondary inductance for each phase is calculated by

$$L_{2Y} = L_{u2} = L_{v2} = L_{w2} = \frac{6}{\pi^2 k\omega}\frac{V_{DC2}^2}{P} \tag{9},$$

where k is the coupling coefficient at the nominal position, ω is the angular transmission frequency. In the proposed system, two transmission coils are connected in series in each phase. Thus, the inductance of each coil is expressed by

$$L_{2Ys} = L_{x2A} = L_{x2B} = \frac{3}{\pi^2 k\omega}\frac{V_{DC2}^2}{P} \tag{10}.$$

Then, the primary inductance is determined. The voltage gain between the primary DC voltage and the secondary DC voltage at the resonant frequency is obtained as

$$\left(\frac{V_{DC2}}{V_{DC1}}\right) = \sqrt{\frac{L_{2Y}}{L_{1Y}}} \tag{11}.$$

From the voltage gain, the primary inductance should be designed by

$$L_{1Y} = L_{u1} = L_{v1} = L_{w1} = \frac{6}{\pi^2 k\omega}\frac{V_{DC1}^2}{P} \tag{12}.$$

In the same manner to the secondary side, because the inductance of each coil is half, the inductance is

$$L_{1Ys} = L_{x1A} = L_{x1B} = \frac{3}{\pi^2 k\omega}\frac{V_{DC1}^2}{P} \tag{13}.$$

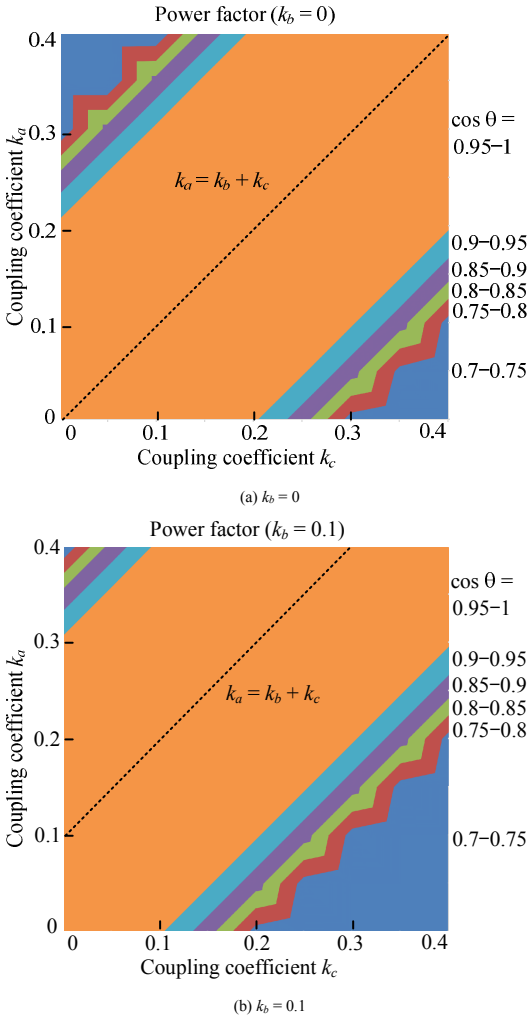

Fig. 4. Effect of the magnetic interference on power factor.

After that, the resonance capacitors are designed. The resonance capacitors are connected in series to the output of the inverter and the input of the rectifier. The resonance capacitors are necessary to compensate the reactive power, which is caused by the weak magnetic coupling between the primary and the secondary side. The resonance capacitors are designed to resonate with the inductance on each phase at the transmission frequency. Consequently, the resonance capacitors on the primary side and the secondary side are calculated by

$$C_{u1Y} = C_{v1Y} = C_{w1Y} = \frac{1}{\omega^2 L_{1Y}} \tag{14},$$

$$C_{u2Y} = C_{v2Y} = C_{w2Y} = \frac{1}{\omega^2 L_{2Y}} \tag{15},$$

respectively. For zero-voltage switching, the transmission frequency is adjusted to be slightly higher than the resonance frequency.

B. Loss Analysis

The power loss of the proposed system including the primary inverter and the rectifier on the secondary side is calculated in this section.

1) Primary Inverter

The primary inverter is operated in square wave operation. The output phase-voltage of the inverter is expressed by

$$V_1 = \frac{\sqrt{2}}{\pi} V_{DC1} \tag{16}.$$

When the power loss can be ignored, the output power is equal to the input power. The primary current I_1 can be derived

$$I_1 = \frac{P}{3V_1} = \frac{\pi P}{3\sqrt{2}V_{DC1}} \tag{17},$$

with the output power P.

The conduction loss of the MOSFETs on the primary inverter is calculated by

$$P_{p\_cond} = 3r_{ds\_on} I_1^2 \tag{18},$$

where r_{ds_on} is the on-resistance of the MOSFETs.

Besides, switching loss is calculated. In IPT systems, the MOSFETs turn-on with zero-voltage switching because the inverter output frequency is adjusted to be slightly higher than the resonant frequency. Therefore, turn-on loss does not occur. By contrast, turn-off loss occurs whereas the output current is sinusoidal. Assuming that sinusoidal current flows on the MOSFETs because the switching frequency is closed to the resonant frequency, the simultaneous current at the turn-off is approximately expressed by

$$i_{sw\_off} = \sqrt{2} I_1 \sin \omega T_d \tag{19},$$

where T_d is the dead time.

The turn-off loss of the primary MOSFETs are calculated by

$$P_{1\_swoff} = 6E_{off(isw\_off)} \frac{V_{DC1}}{V_n} \times f_{sw} \tag{20},$$

where E_{off} is the turn-off energy, and V_n is the drain-source voltage when the turn-off energy is measured.

2) Secondary Rectifier

The secondary current is calculated by

$$I_2 = \frac{\pi P}{3\sqrt{2}V_{DC2}} \tag{21},$$

in the same manner to the primary side. The secondary current flows on the diodes during half the period. Thus, the conduction loss of the secondary diodes are calculated by

$$P_{2\_Dcond} = 6\frac{1}{T}\int_0^{\frac{T}{2}} V_F \sqrt{2} I_2 \sin \omega t dt = \frac{6\sqrt{2}V_F I_2}{\pi} \tag{22},$$

where V_F is the forward voltage drop of the each diode.

3) Transmission Coils

The copper loss of the primary coils and the secondary coils are calculated by

$$P_{1\_copper} = r_1 I_1^2 \tag{23},$$

$$P_{2\_copper} = r_2 I_2^2 \tag{24},$$

respectively with the winding resistances r_1 and r_2.

Then, iron loss of the transmission coils is derived from the magnetic flux density using the datasheet of the ferrite core because the current on the transmission coils are sinusoidal. In this consideration, it is assumed that the magnetic flux density on the core is uniform. The magnetic flux density of the primary coils and the secondary coils is calculated by

$$B_1 = \frac{L_{Y1s} I_1 + M I_2}{N_1 S_1} \tag{25},$$

$$B_2 = \frac{L_{Y2s} I_2 + M I_1}{N_2 S_2} \tag{26},$$

where N_1 and N_2 are the numbers of turns of the windings, and S_1 and S_2 are the cross section of the ferrite core. The iron loss can be calculated from the datasheet based on the magnetic flux density.

IV. Experimental Verification

A. Experimental Setup

The proposed three-phase IPT system is tested with a 2.9-kW prototype. Fig. 5 shows the transmission coils. The transmission coils are circularly placed and adjusted the distance among them to satisfy the cancellation condition of the magnetic interference derived as (6–7). The magnetic interference among the coils are k_a = 0.048, k_b = 0.011, and k_c = 0.003. Other parameters are shown in Table I.

Figure 6 shows the definition of the rotational coil misalignment. Fig. 7 shows the parameter change by coil misalignment. Due to the rotation misalignment, the inductance of the coils and the coupling coefficient is changed. In Fig. 6, the inductance and the coupling coefficient are normalized based on the value without a misalignment. Note that the coupling coefficient between primary and secondary coils, which are closest, are indicated. When the rotational angle is 30 degrees, the inductance and the coupling coefficient are minimal. The inductance and the coupling coefficient are reduced by 3.4% and 52.4% at a maximum. However, the effect of the coupling coefficient is symmetry owing to the coil placement. If the rotational misalignment is larger than 30 degrees, the primary coil transmits power to another phase, e.g., from L_{u1A} to L_{v2B}.

(a) Three-phase SiC inverter

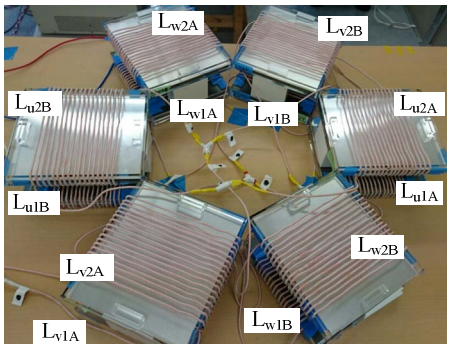

(b) Transmission coils

Fig. 5. 2.9-kW prototype.

TABLE I. Specification of 2.9-kW Prototype

Parameters				
Output power		P	2.9	kW
DC voltage	Primary	V_{DC1}	400	V
	Secondary	V_{DC2}	400	V
Switching frequency		f_{sw}	85.5	kHz
Coupling coefficient		k	0.25	
Inductance (at nominal position)	Primary	L_{u1A}	107.1	μH
		L_{u1B}	107.9	μH
		L_{v1A}	106.9	μH
		L_{v1B}	104.2	μH
		L_{w1A}	106.5	μH
		L_{w1B}	109.7	μH
	Secondary	L_{u2A}	108.0	μH
		L_{u2B}	107.0	μH
		L_{v2A}	109.4	μH
		L_{v2B}	107.6	μH
		L_{w2A}	106.3	μH
		L_{w2B}	105.6	μH
Capacitance (average)	Primary	C_1	16.4	nF
	Secondary	C_2	16.4	nF
Dead time		T_d	250	ns
Number of turn	Primary	N_1	17	turn
	Secondary	N_2	17	turn
Wire		Litz 2UEWSTC 784 / ϕ0.1		
MOSFETs		SCT3030AL (ROHM)		
Diodes		VS-20ETF0 (Vishay)		

B. Experimental Results

Figure 8 shows the operation waveforms. The output current is 30 degrees lagging from the output line voltage v_{uv1}. Thus it is confirmed that the proposed IPT system is operated at the resonant frequency without the effect of the magnetic interference. Moreover, the inverter output current is equilibrium.

Figure 9 shows the radiation noise measured at 2 m from the edge of the coils. The radiation noise is compared with the conventional three-phase six coil IPT system, i.e., the coils L_{xnB} are removed. The noise is measured with common conduction current on the coils. The radiation noise at the fundamental frequency is suppressed from 12.2 dBμA to 2.1 dBμA.

Figure 10 shows the DC-to-DC efficiency characteristic. The efficiency is evaluated with changing load resistance. Thus, the output voltage is also changed. The maximum DC-to-Dc efficiency is 90.6% at an output power of 2.9 kW (input power is 3.2 kW). Note that the output power is changed by changing the load resistance in this experiment. It means that the output voltage is not constant.

Figure 11 shows the comparison of the power loss between the calculation, which is calculated using the equation in chapter III, and the measured loss. The measured power loss is 304 W whereas the calculation is 282 W. The calculation result shows a good agreement with the experimental value with an error of 7.3%. The dominating power loss is the copper loss of the primary coil and the secondary coil. The sum of the copper loss accounts for about 80% of the total power loss. The system efficiency will be improved by reducing an AC resistance of the wire using more thick litz wire.

Figure 12 shows the calculation result on the power loss of the 22-kW proposed IPT system. Because the IPT system with an input power of more than 22 kW will be standardized [5–6], 22-kW IPT system is evaluated. The

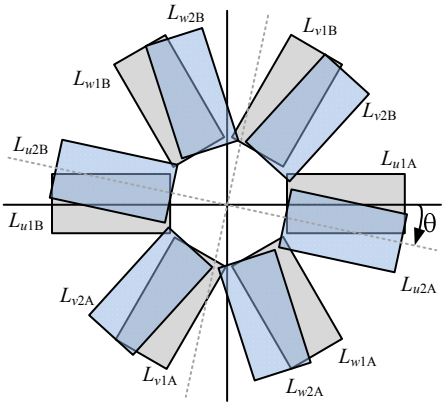

Fig. 6. Assumed rotational coil misalignment.

calculation conditions are shown in Table II. The major difference between the 2.9-kW system is the input and output DC voltage. The input voltage is increased from 400 V to 800 V. Moreover, 1200-V SiC-MOSFETs are used for high voltage input DC. A DC-to-DC efficiency of 93.7% will be obtained.

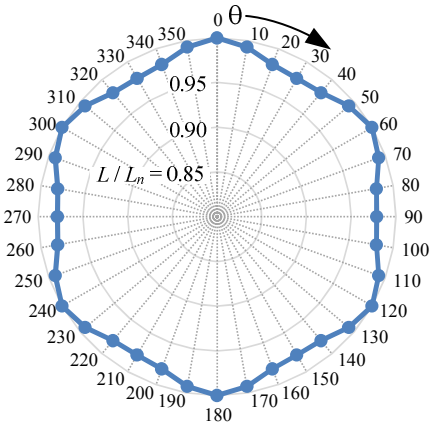

(a) Self-inductance of primary coils

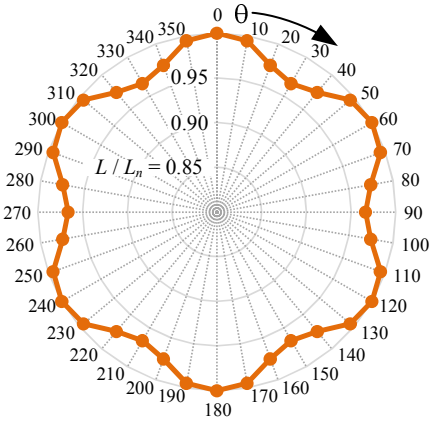

(b) Self-inductance of secondary coils

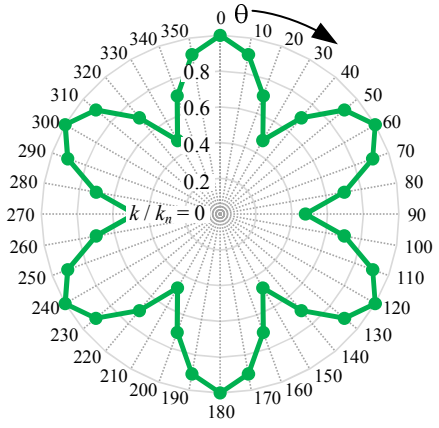

(c) Coupling coefficient

Fig. 7. Indutance and coupling coefficient change due to the rotationl coil misalignment. The indutance and coupling coefficient are normalized by the value without a coil misalignment.

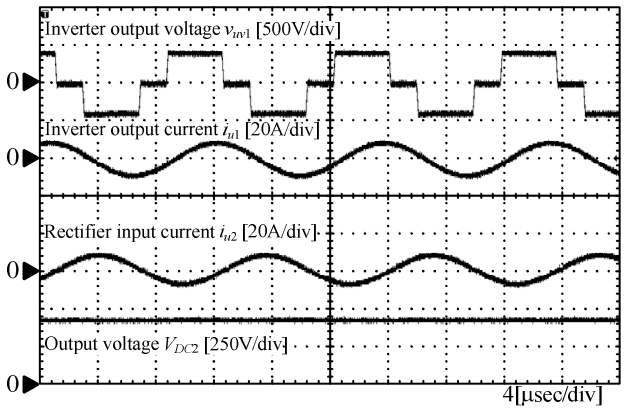

(a) Inverter output voltage, output current, rectifier input current, and output voltage

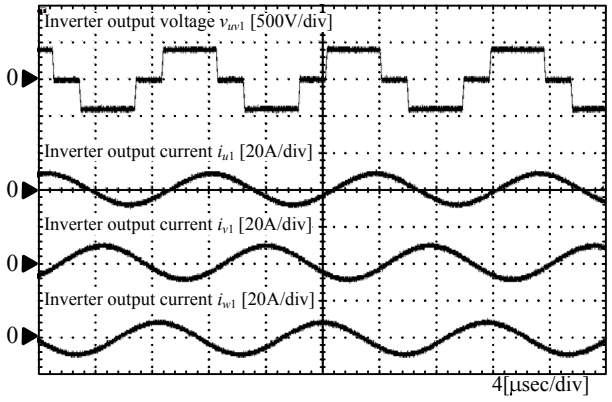

(b) Inverter output voltage, output current on the primary coil

Fig. 8. Operation waveforms.

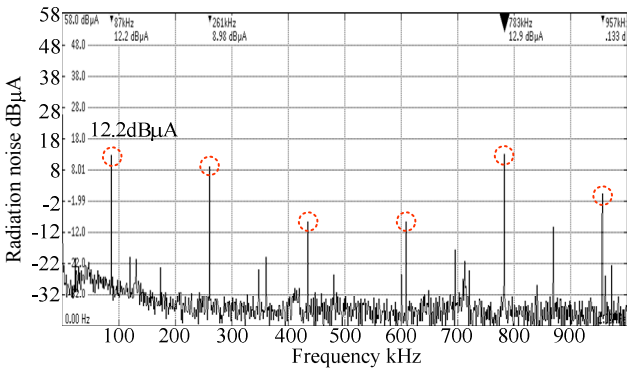

(a) Conventional system (six coils)

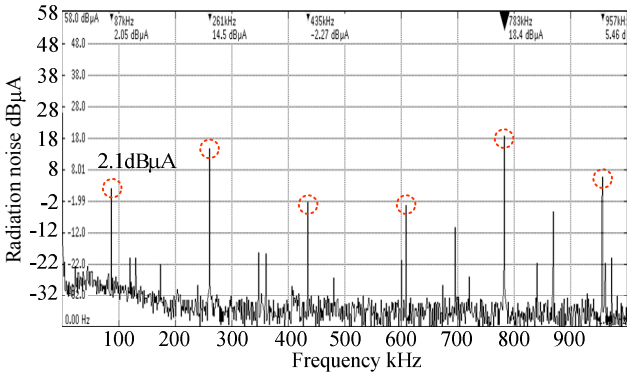

(b) Proposed system (12 coils)

Fig. 9. Radiation noise at 2m from the coil edge.

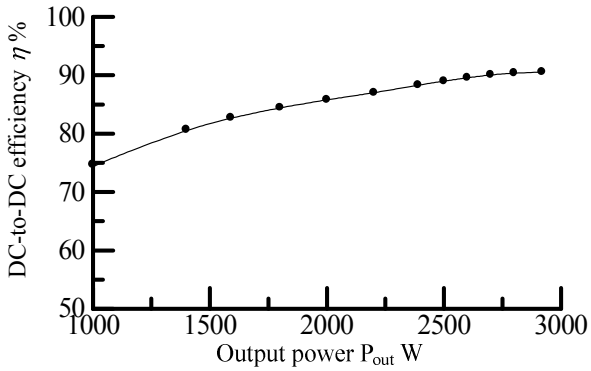

Fig. 10. Efficiency characteristic.

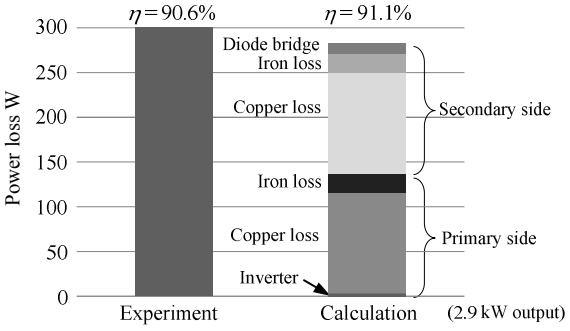

Fig. 11. Power loss separation of 2.9-kW prototype.

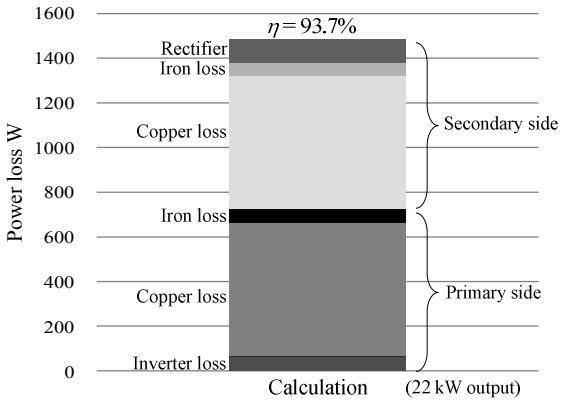

Fig. 12. Power loss calculation of a 22-kW IPT system.

TABLE II. SPECIFICATION OF 22-KW IPT SYSTEM.

Parameters				
Output power		P	22	kW
DC voltage	Primary	V_{DC1}	800	V
	Secondary	V_{DC2}	800	V
Switching frequency		f_{sw}	85.5	kHz
Coupling coefficient		k	0.25	
Inductance (at nominal position)	Primary	L_{1s}	16.5	μH
	Secondary	L_{2s}	16.5	μH
Capacitance (average)	Primary	C_1	14.4	nF
	Secondary	C_2	14.4	nF
Dead time		T_d	250	ns
Number of turn	Primary	N_1	6	turn
	Secondary	N_2	6	turn
MOSFETs	BSM080D12P2C008 (Rohm)			
Diodes	DSEP2x31-12A (IXYS)			

V. CONCLUSION

In this paper, the three-phase IPT system with 12 coils for radiation noise reduction is proposed. The three-phase IPT system cancels out the radiation noise with two series-connected solenoid-coils. Moreover, six primary coils and six secondary coils capable of canceling out the magnetic interference among these coils. Thus, the proposed system can be dealt as six independent single-phase IPT system. The 2.9-kW IPT system is demonstrated. The radiation noise at the fundamental frequency is reduced from 12.2 dBμA to 2.1 dBμA. Moreover the power loss is analyzed. The calculation result shows good agreement with the experimental value with an error of 7.3%. Finally, the 22-kW IPT system with the proposed topology is estimated. The estimated DC-to-DC efficiency is 93.7%.

REFERENCES

[1] K. Kusaka. J. Itoh, "Development Trends of Inductive Power Transfer Systems Utilizing Electromagnetic Induction with Focus on Transmission Frequency and Transmission Power," IEEJ Journal of Industry Applications, Vol. 6, No. 5, pp. 328-339 (2017)

[2] R. Bosshard, J. W. Kolar, B. Wunsch: "Accurate Finite-Element Modeling and Experimental Verification of Inductive Power Transfer Coil Design," IEEE Applied Power Electronics Conference and Exposition 12th, Vol. , No. , pp. 1648-1653 (2014)

[3] G. Lovison, D. Kobayashi, M. Sato, T. Imura, and Y. Hori, "Secondary-side-only Control for High Efficiency and Desired Power with Two Converters in Wireless Power Transfer Systems," IEEJ Journal of Industry Applications, Vol. 6, No. 6, pp. 473-481 (2017)

[4] T. Koyama, K. Umetani, and E. Hiraki, "Design Optimization Method for the Load Impedance to Maximize the Output Power in Dual Transmitting Resonator Wireless Power Transfer System," IEEJ Journal of Industry Applications, Vol. 7, No. 1, pp. 49-55 (2018)

[5] International Organization for Standardization, "Electrically propelled road vehicles — Magnetic field wireless power transfer — Safety and interoperability requirements," Publicly available specification: ISO/PAS19363:2017(E)

[6] International Electrotechnical Commission, "Electric vehicle wireless power transfer (WPT) systems – Part 1: General requirements," International standard: IEC 61980-1 (2015)

[7] International Special Committee on Radio Interference, "Industrial, scientific and medical equipment — Radio-frequency disturbance characteristics — Limits and methods of measurement," CISPR 11: 2015 (2015)

[8] Kent Inoue, Keisuke Kusaka, Jun-ichi Itoh: "Reduction in Radiation Noise Level for Inductive Power Transfer Systems using Spread Spectrum Techniques," IEEE Trans. on Power Electronics, Vol. 33, No. 4, pp. 3076-3085 (2018)

[9] T. Shijo, K. Ogawa, M. Suzuki, Y. Kanekiyo, M. Ishida, and S. Obayashi, "EMI Reduction Technology in 85 kHz Band 44 kW Wireless Power Transfer System for Rapid Contactless Charging of Electric Bus," IEEE Energy Conversion Congress & Expo 2016, No. EC-0641 (2016)

[10] T. Shijo, K. Ogawa, F. Moritsuka, M. Suzuki, H. Ishihara, Y. Kanekiyo, K. Ogura, M. Ishida, S. Obayashi, S. Shimmyo, K. Maki, F. Takeuchi, and N. Tada, "85 kHz band 44 kW wireless power transfer system for rapid contactless charging of electric bus," International Symposium on Antennas and Propagation 2016, pp. 38-39 (2016)

[11] Y. H. Sohn, B. H. Choi, E. S. Lee, G. C. Lim, G. Cho, and C. T. Rim: "General Unified Analyses of Two-Capacitor Inductive Power Transfer Systems: Equivalence of Current-Source SS and SP Compensations," IEEE Trans. On Power Electronics, Vol. 30, No. 11, pp. 6030-6045 (2015)

[12] R. L. Steigerwald, "A Comparison of Half-Bridge Resonant Converter Topologies," IEEE Trans. Power Electron. Vol. 3, no. 2, pp. 174-182, Apr. 1988.